COLLIMATOR IRRADIATION STUDIES AT THE ADVANCED PHOTON SOURCE*

J. Dooling[†], W. Berg, M. Borland, J. Calvey, L. Emery, A. Grannan, K. Harkay, Y. Lee,
R. Lindberg, G. Navrotski, V. Sajaev, N. Sereno, J. Stevens, Y. Sun, K. P. Wootton
Argonne National Laboratory, Lemont, Illinois, USA
N. Cook, RadiaSoft LLC, Boulder, Colorado, USA
D. Lee, S. Riedel, University of California, Santa Cruz, Santa Cruz, California, USA

Abstract

We present results from a recent collimator irradiation experiment conducted in the Advanced Photon Source (APS) storage ring. This experiment is the third in a series of studies to examine the effects of high-intensity electron beams on potential collimator material for the APS-Upgrade (APS-U). The intent here is to determine if a fan-out kicker can sufficiently reduce e-beam power density to protect horizontal collimators planned for installation in the APS-U storage-ring. The fan-out kicker (FOK) spreads the bunched-beam vertically allowing it to grow in transverse dimensions prior to striking the collimator. In the present experiment, one of the two collimator test pieces is fabricated from oxygen-free copper; and the other is from 6061-T6 aluminum. As in past studies, diagnostics include turn-by-turn BPMs, a diagnostic image system, fast beam loss monitors, a pin-hole camera, and a current monitor. Post-irradiation analyses employ microscopy and metallurgy. To avoid confusion from multiple strikes, only three beam aborts are carried out on each of the collimator pieces; two with the FOK on and the other with it off. Observed hydrodynamic behavior will be compared with coupled codes.

INTRODUCTION

Previous whole-beam-loss experiments carried out in 2019 and 2020 in the Advanced Photon Source (APS) storage ring (SR) studied effects in aluminum and titanium collimator test pieces [1–3]. No steps were taken to mitigate damage caused by the high intensity electron beam during these earlier studies. In the present experiment, a vertically-deflecting fan-out kicker (FOK) was employed to spread the beam bunch train transversely on both aluminum and copper targets. The action of the FOK spreads both the bunch train as well as individual bunches; in the latter case, by forcing them into regions of non-linear focusing.

Unlike earlier collimator experiments, where studies were carried out at the beginning of a user run, this study took place during the final Machine Studies period at the end of APS SR operations. The collimator test pieces were installed for the entire final run and thus were well conditioned for the experiment.
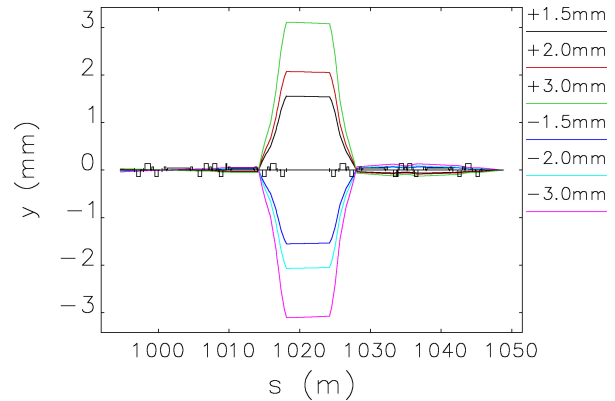
Figure 1: Vertical bumps in the Sector 37 region modeled with `elegant`.

Table 1: Beam Abort Case List Parameters

Case No.	Vertical Offset (mm)	Mat'l	FOK Voltage (kV)	Vertical Defl. Angle y' (µrad)
0	+1.5	Cu	2	245.0
1	-1.5	Al	2	245.0
2	-2.0	Al	1	122.5
3	+3.0	Cu	0	0
4	-3.0	Al	0	0
5	+2.0	Cu	3	367.5

EXPERIMENTAL DESCRIPTION

As in previous experiments, the collimator test piece targets were placed in the Sector 37 (S37) straight section approximately 2 m downstream of the fourth S37 rf cavity. Vertical orbit bumps in the S37 region used to separate the strike regions on the targets were simulated with `elegant` [4, 5] and shown in Fig. 1. With positive y-bumps, the beam strikes copper and with negative bumps, the beam intercepts aluminum.

Six separate whole-beam aborts with 200 mA, 6 GeV beam were employed to strike the collimator test pieces; three on the copper and three on the aluminum. The six cases are summarized in Table 1.
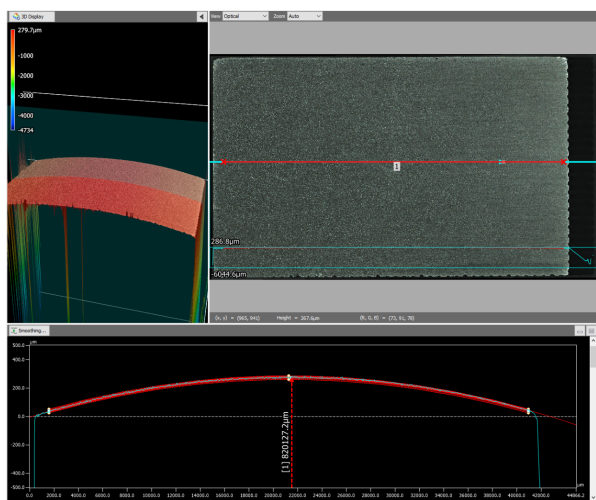
Figure 2: Surface images and profile obtained with a Keyence VR3200 microscope for the Al test piece.

Figure 3: Copper test piece showing 1-mm-spaced rulings on the gap side.

MEASUREMENTS

Pre-Studies

Surface analysis was performed on each of the test pieces. An 80 cm radius was machined into each of the pieces beam-facing surfaces; this relatively large radius resulted in a 0.28 mm peak height above the chord connecting the upstream and downstream ends as shown in Fig. 2 for the aluminum piece. These images were recorded using a Keyence VR3200 microscope. The peak or apex is where we expect the beam to strike first during a loss event. The full length of the chord from the upstream to downstream edges of the beam-facing collimator surface is 41 mm.

For fiducialization and wakefield studies, 1 mm-spaced rulings were machined on the side of the copper piece facing the gap, see Fig. 3. Rulings were also added to the aluminum piece, but not on the gap side. The rulings depths were nominally specified as 0.127 mm (5 mils); for every fifth ruling, the depth was specified as 0.254 mm or 10 mils.
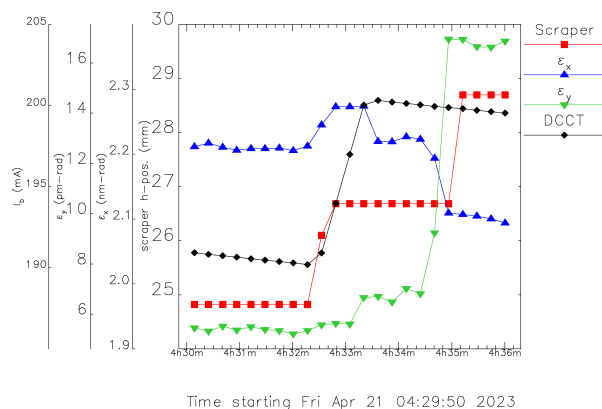

Figure 4: Case 0 horizontal and vertical emittances as the collimators are positioned for the dump. Scraper refers to the horizontal position of the collimator apex; at h-pos = 30.85 mm, the apex is nominally at chamber centerline.
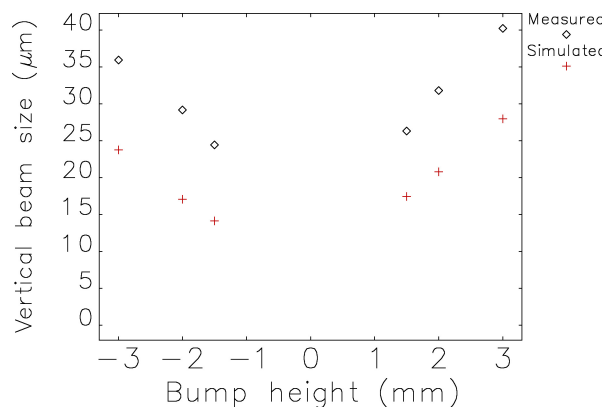

Figure 5: Predicted and measured vertical beam sizes.

Studies

A total of six whole-beam dumps were conducted. All six loss events were carried out with stored beam current of 200 mA and a 972-bunch fill pattern. The whole-beam loss events are initiated by muting the rf drive once the collimator test pieces were in place.

Pinhole Camera The S35 pinhole camera is an important diagnostic providing horizontal and vertical beam sizes which in turn provide beam emittances when combined with machine lattice functions. Sextupole magnets within the bump were inadvertently left powered during the beam abort study which led to an planned increase in vertical emittance. An example of the growth in vertical emittance is shown for case 0 in Fig. 4 as the collimators are moved toward the horizontal parking position for beam dumps. The plot ends with the beam dump. The apex of the collimators are nominally placed 2 mm from the beam centerline prior to initiating a beam abort corresponding to h-pos=28.85 cm. Predicted and measured vertical sizes for the six cases presented here are plotted in Fig. 5.
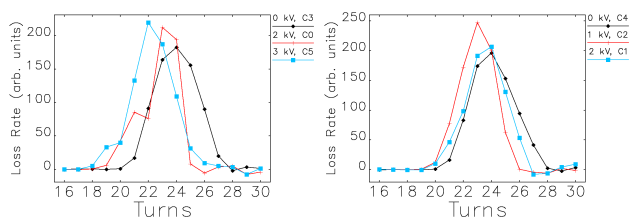
Figure 6: Measured loss rates in the copper (left) and aluminum collimator test pieces.
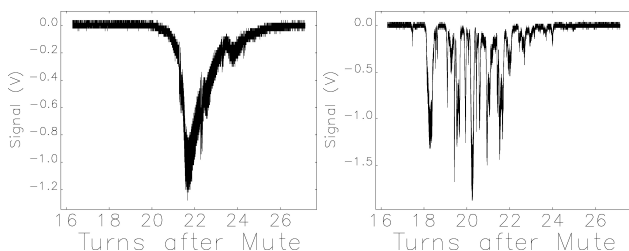

Figure 7: Fast fiber optic beam loss signals in S6 for Cases 3 (FOK=0 kV, left) and 5 (FOK=3 kV).

Turn-by-Turn BPMs Differentiated sum signals from the turn-by-turn (TBT) BPMs provide the loss rate during the whole-beam loss events. Measured loss rates from the TBT BPMs are plotted in Fig. 6. Based on `elegant` simulations for APS-U, FOK voltages should be kept less than 3 kV.

Fast Fiber Optic Beam Loss Monitors Fast fiber-optic beam loss monitors (FOBLM) provide intra-turn loss information. With a rise-time of approximately 2 ns, the FOBLM is not fast enough to resolve the losses from individual bunches in a 972-bunch fill pattern (1296 buckets at 352 MHz, with 3 of 4 buckets filled), the diagnostic can observe time-averaged behavior. In Fig. 7 losses in S6 are shown for Cases 3 and 5 (FOK=0 and 3 kV). Large variations in the loss signal is seen for the 3 kV case. These large fluctuations are not desirable and can lead to losses outside the collimator regions.

Diagnostic Imaging System Immediately following the whole-beam-loss study an image was acquired of the upstream end of the collimator surfaces. The image shown in Fig. 8 shows the effects of the six strikes listed in Table 1.

Post Studies

Gamma Spectroscopy Radiation monitors indicated the copper test piece to be activated. Gamma spectroscopy found approximately 135 pCi of cobalt-57. Gamma spec measurements were conducted over an integration time of 1 hour on July 27, 2023 roughly 3 months after irradiation. No activation was indicated in the aluminum piece.

Photography Photographs of the collimator beam-facing surfaces are presented in Fig. 9. The orientation of the two images is similar to the arrangement of the collimator
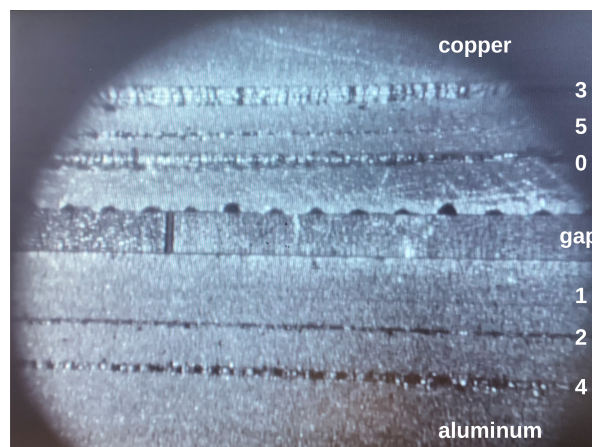

Figure 8: Image of the upstream end of the collimator surfaces after whole-beam strikes. Numbering refers to the Cases list in Table 1.
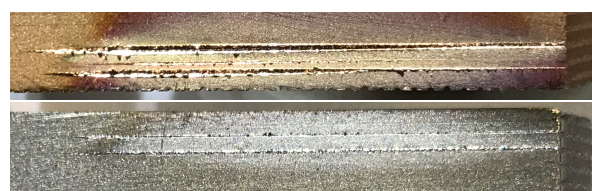

Figure 9: Photographs of strike regions in copper (top) and aluminum. Beam was moving from right to left.

test pieces when mounted during the experiment. In Fig. 9 the full length of the damaged region (3.3 cm) is shown; whereas in Fig. 8, the image covers only the upstream region of the mounted pieces with a 11 mm field of view.

Metallurgy Though we do not yet have access to the test pieces used for the April 2023 study, metallurgical analysis has been performed on the aluminum pieces irradiated during the January 2020 experiment [1]. After cutting and polishing to 0.05 μm, the color tinting chemical etchant "Weck's Reagent" was used by immersion for 30 seconds to highlight micro-segregation of different phases in aluminum, especially to differentiate the melted, heat affected and unaffected base metal properties of the irradiated regions. An example of this analysis is shown in Fig. 10. Under polarized lighting, the melt regions generally have a green tint highlighting turbulent mixing present during the rapid melting and solidification process. The orange color highlights unaffected aluminum alloy base metal. Close inspection shows a heat affected but non-melted zone between the two regions. (Grey/black areas are encapsulating plastic used to preserve surface features.) The double beam-strike image shows metal ejection and re-solidification onto open surfaces.
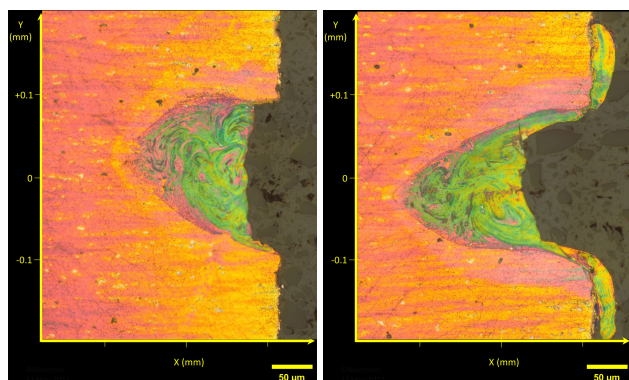
Figure 10: Metallurgical analysis of irradiated aluminum test piece cross sections from January 2020. Single strike at 200 mA (left) and double strikes at 200 mA (right). The images are from separate y-position strike locations.
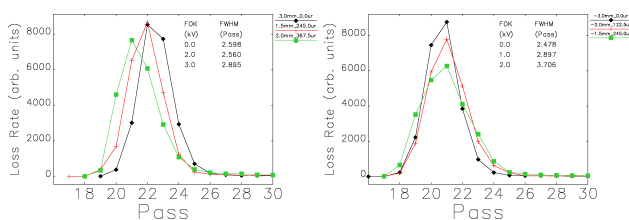

Figure 11: Simulated loss rates in the copper (cases 3, 0, 5; left) and aluminum (cases 4, 2, 1) collimator test pieces. Refer to Table 1 for case numbers.

SIMULATIONS

Dose Distributions with `elegant` and MARS

Plots of `elegant`-derived loss rates for strikes on aluminum and copper test pieces are presented in Fig. 11. These temporal profiles can be compared with the measured loss rates shown in Fig. 6. We observe that the loss duration appears to increase with FOK voltage for the simulated loss rates; this trend is not evident in the measured TBT data.

The x-integrated `elegant`-generated transverse loss distributions (all Passes) are presented in Fig. 12 for strikes on aluminum with FOK voltage settings of 0, 1, and 2 kV. These and the other four distributions will be used as input for MARS [6] to generate temporal dose distributions with a time increment of 1 turn or pass (3.68 μs) [7]. The dose distributions are in turn used as input to the hydrodynamics code, FLASH [8]. Figure 12 shows significant spreading of the loss with 2 kV on the FOK relative to the 0 voltage case.

Simulating Liquid Phase with FLASH

Simulations of damage to collimator materials done with the FLASH hydrodynamics code [8] have thus far not included any modeling of a "liquid phase". Instead, the collimator material in each cell is treated as a solid and is not evolved by FLASH until the electron temperature, T_{ele}, in that cell exceeds a threshold temperature, $T_{thresh} = 4115$ K for Al, and 4252.5 K for Cu).
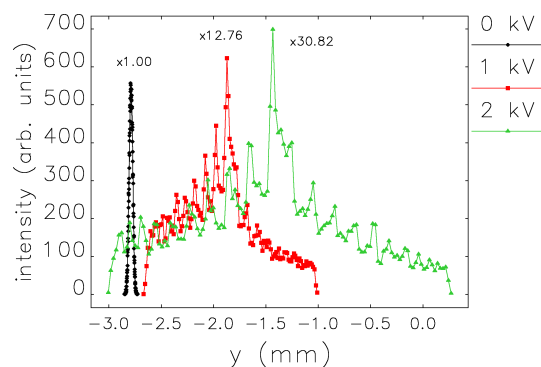
Figure 12: Simulated x-integrated y-loss intensity distributions on aluminum based on measured emittance for FOK voltages of 0, 1, and 2 kV. Using 0 kV as the reference, the amplitudes of the 1 and 2 kV profiles are increased by factors of 12.76 and 30.82 indicating the reduction of intensity the FOK provides.

We plan to begin modeling the liquid phase, first for copper and then for aluminum. The first step will be to replace the constant thermal conductivity model for solid phase copper (which is currently being used) with a more accurate model in the temperature range $0K < T_{ele} \leq T_{melt,Cu}$ where $T_{melt,Cu} \approx 1358$ K is the melting point of copper [9]. Then a new phase transition from solid to liquid will be added at $T_{ele} = T_{melt,Cu}$. This first implementation will focus be on more accurately modeling the density [10], thermal conductivity [11], and specific heat of liquid copper in the temperature range of $T_{melt,Cu} \leq T_{ele} \leq T_{thresh}$. The phase transition to plasma will still occur at $T_{thresh} = 4252.5$ K

In preliminary simulations, adding a liquid phase has helped avoid nonphysical "islands" of solid copper that are not connected to the main collimator material. It also allows the vaporized copper to re-liquefy from the plasma phase, a feature not previously implemented. Eventually we hope to be able to evolve the state of the liquid phase collimator material using the hydrodynamics capabilities of FLASH.

SUMMARY

A third whole-beam-abort experiment was conducted to study whether a vertical FOK could be utilized to protect the horizontal collimators planned for the APS-U SR. Tests were carried out on both aluminum and copper targets. In the case of aluminum, a FOK voltage of 2 kV was sufficient to protect the target; however, for copper even a 3 kV kick was not enough to prevent damage. For both targets, damage was reduced as FOK voltage was increased. The data collected will provide useful information for benchmarking our coupled-code simulation effort modeling the effects of whole-beam loss events in fourth generation light sources.

ACKNOWLEDGMENTS

REFERENCES

[1] J. Dooling *et al.*, "Collimator irradiation studies in the argonne advanced photon source at energy densities expected in next-generation storage ring light sources," *Phys. Rev. Accel. Beams*, vol. 25, no. 4, p. 043 001, 2022. `doi:10.1103/PhysRevAccelBeams.25.043001`

[2] J. C. Dooling *et al.*, "Diagnostics for Collimator Irradiation Studies in the Advanced Photon Source Storage Ring," in *Proc. IBIC'20*, Santos, Brazil, Sep. 2020, pp. 26–33. `doi:10.18429/JACoW-IBIC2020-TUAO02`

[3] J. C. Dooling *et al.*, "Studies of Beam Dumps in Candidate Horizontal Collimator Materials for the Advanced Photon Source Upgrade Storage Ring," in *Proc. NAPAC'19*, Lansing, MI, USA, Sep. 2019, pp. 128–131. `doi:10.18429/JACoW-NAPAC2019-MOPLM14`

[4] M. Borland, "elegant: A Flexible SDDS-Compliant Code for Accelerator Simulation," Advanced Photon Source, Tech. Rep. LS-287, 2000. `doi:10.2172/761286`

[5] Y. Wang and M. Borland, "Implementation and Performance of Parallelized Elegant," in *Proc. PAC'07*, Albuquerque, NM, USA, Jun. 2007, pp. 3444–3446. `doi:10.1109/PAC.2007.4440453`

[6] N. V. Mokhov, "The Mars Code System User's Guide," Fermilab, FN 628, 1995. `doi:10.2172/1987276`

[7] J. C. Dooling *et al.*, "Hydrodynamic and Beam Dynamic Simulations of Ultra-Low Emittance Whole Beam Dumps in the Advanced Photon Source Storage Ring," in *Proc. NAPAC'22*, Albuquerque, NM, USA, 2022, pp. 390–393. `doi:10.18429/JACoW-NAPAC2022-TUPA21`

[8] B. Fryxell *et al.*, "FLASH: An adaptive mesh hydrodynamics code for modeling astrophysical thermonuclear flashes," *Astrophys. J. Suppl. Ser.*, vol. 131, no. 1, p. 273, 2000. `doi:10.1086/317361`

[9] J. G. Hust and A. B. Lankford, "Thermal Conductivity of Aluminum, Copper, Iron, and Tungsten for Temperatures from 1 K to the melting point," National Institute of Standards and Technology, U.S. Department of Commerce, Boulder, Colorado, Tech. Rep. NBSIR 84-3007, 1984, pp. 4–15. `https://www.govinfo.gov/content/pkg/GOVPUB-C13-5dca61206b094d8b3a54099ebcff1baa/pdf/GOVPUB-C13-5dca61206b094d8b3a54099ebcff1baa.pdf`

[10] J. A. Cahill and A. D. Kirshenbaum, "The density of liquid copper from its melting point (1356 K to 2500 K and an estimate of its critical constants1,2," *J. Phys. Chem.*, vol. 66, no. 6, pp. 1080–1082, 1962. `doi:10.1021/j100812a027`

[11] M. Assael, A. Chatzimichailidis, K. Antoniadis, W. Wakeham, M. Huber, and H. Fukuyama, "Reference correlations for the thermal conductivity of copper, gallium, indium, iron, lead, nickel and tin," *High Temp.-High Pressures*, no. 46, 2017.